



Hierarchical CoP/Ni₅P₄/CoP microsheet arrays as a robust pH-universal electrocatalyst for efficient hydrogen generation

Journal:	<i>Energy & Environmental Science</i>
Manuscript ID	EE-ART-05-2018-001270.R1
Article Type:	Paper
Date Submitted by the Author:	24-May-2018
Complete List of Authors:	Mishra, Ishwar; University of Houston, Department of Physics Zhou, Haiqing; University of Houston, Department of Physics; Hunan Normal University, School of Physics and Electronics Sun, Jingying ; University of Houston, Physics & Texas center for superconductivity Dahal, Keshab; University of Houston, Physics Chen, Shuo; University of Houston, Physics Ren, Zhifeng ; University of Houston, Physics



Energy & Environmental Science

Paper

Hierarchical CoP/Ni₅P₄/CoP microsheet arrays as a robust pH-universal electrocatalyst for efficient hydrogen generation

Received 00th January 20xx,
Accepted 00th January 20xx

Ishwar Kumar Mishra,^{†a} Haiqing Zhou,^{†a,b} Jinying Sun,^a Keshab Dahal,^a Shuo Chen^{*a} and Zhifeng Ren^{*a}

DOI: 10.1039/x0xx00000x

www.rsc.org/

Highly active catalyst composed of earth-abundant materials performing as efficient as Pt catalysts is crucial for sustainable hydrogen production through water splitting. However, most efficient catalysts are made of nanostructures by complex synthetic methods, making it quite challenging for scale-up. Here we report an effective strategy to develop a very active and durable pH-universal electrocatalyst for hydrogen evolution reaction (HER). This catalyst is constructed by a sandwich-like structure where hierarchical cobalt phosphide (CoP) nanoparticles serve as the thin skins covering both sides of nickel phosphide (Ni₅P₄) nanosheet arrays, forming self-supported sandwich-like CoP/Ni₅P₄/CoP microsheet arrays with lots of mesopores and macropores. The as-prepared electrocatalyst requires an overpotential of only 33 mV to achieve the benchmark 10 mA cm⁻² with very large exchange current density, and high turnover frequencies (TOFs) in acid media, which is superior to most electrocatalysts made of metal phosphides, well-known MoS₂, and WS₂ catalysts, and performs as comparably as the state-of-the-art Pt catalysts. In particular, this electrocatalyst shows impressive operational stability at extremely large current densities of 1 A cm⁻², indicating its possible application toward large-scale water electrolysis. Additionally, this electrocatalyst is very active in alkaline electrolyte (71 mV at 10 mA cm⁻²), which demonstrates its pH universality as a HER catalyst with outstanding catalytic activity. This simple strategy does not involve any solvothermal and hydrothermal process, paving a new avenue to design robust non-noble electrocatalysts for hydrogen production toward commercial water electrolysis.

Hydrogen produced by water electrolysis is a clean energy carrier, which can be regarded as a potential alternative to fossil fuels.¹⁻⁴ Water dissociation for hydrogen production via electrolysis requires highly active catalysts to minimize the overpotentials. Platinum (Pt)-based materials are the most active electrocatalysts for hydrogen

Broader context

Hydrogen is an ideal energy carrier to replace carbon-containing fuels due to its high energy density and zero pollution gas emission. Water electrolysis is very appealing to produce hydrogen in large scale with low cost, high purity and renewability, but it requires robust and stable electrocatalysts to expedite the reaction kinetics. On earth, there are various water sources including acidic, alkaline, industrial waste water, and seawater with different pH values, possible for hydrogen production. In fact, there are many water electrolysis technologies with different demands on the pH values of the electrolytes, including proton exchange membrane electrolysis in strong acid, microbial electrolysis and sea-water electrolysis in neutral solutions, and commercially used water electrolysis in base. Thus, developing efficient and cheap electrocatalysts operating well at wide pH solutions for hydrogen evolution is highly desirable. Here we introduce an effective approach to develop an active and durable pH-universal electrocatalyst constructed by CoP/Ni₅P₄/CoP microsheet arrays forming a sandwich-like structure. This electrocatalyst is very active for hydrogen evolution in strong acid and base, showing good durability at large current densities. This discovery paves a new avenue toward the rational design of robust non-noble metal-containing electrocatalysts for water splitting.

evolution reaction (HER). However, the noble-metal based catalysts are not suitable for large-scale application due to their high cost and limited availability on the earth's crust.^{5,6} For sustainable and clean hydrogen economy, highly active and affordable catalysts based on earth-abundant materials have to be developed.

Noble metal-free materials including metal sulfides, selenides, phosphides, etc., have been widely explored for catalyzing HER.⁷⁻¹⁰ Among them, transition-metal phosphides (TMPs) have been receiving significant attention due to their promising catalytic activity for HER in water splitting.^{11,12} In the past years, several efficient TMP-based materials have been explored for HER, including Ni₂P,¹⁰ Mo-W-P,¹³ CoP/CC,¹⁴ CoPS,¹⁵ and Fe_xCo_{1-x}P.¹⁶ Despite considerable achievements, it still remains a big challenge to design and develop catalysts consisting of earth-abundant materials with Pt-like pH-universal HER activity and promising operational stability at high current densities (> 500 mA cm⁻²)

^aDepartment of Physics and TcSUH, University of Houston, Houston, TX 77204, United States. Email: schen34@uh.edu, zren@uh.edu

^bSchool of Physics and Electronics, Hunan Normal University, Changsha 410081, China.

[†]These authors contributed equally to this work.

[†]Electronic Supplementary Information (ESI) available: experimental details and results. See DOI: 10.1039/x0xx00000x

considering not good long-term stability of Pt catalysts in both acidic and alkaline media.¹⁷ Indeed, little attention has been given to their structural design to enhance the catalytic activity and long-term durability especially at even higher current densities ($> 2 \text{ A cm}^{-2}$), which is crucial for large-scale hydrogen production through electrocatalytic water splitting. Especially, many catalysts involve complicated preparation procedures, which are not industrially compatible. What's more, an ideal electrocatalyst is expected to exhibit outstanding catalytic HER activity over a wide pH range (0–14) like Pt, considering the abundant sources of water on earth, and different water electrolysis technologies with different demands on the pH values of the electrolytes.^{14,18,19} However, very few non-noble electrocatalysts can be simultaneously robust in catalyzing the HER in both acidic and alkaline media. Thus, developing robust catalysts with pH universality and long-term durability at high current densities remains challenging. In this work, we report a rational design of a highly active electrocatalyst based on a sandwich-like hybrid of cobalt and nickel phosphides for HER in water splitting. The cobalt phosphide (CoP) nanoparticles were designed to cover nickel phosphide (Ni_5P_4) nanosheet arrays, forming self-supported microsheet arrays. Benefiting from the sandwich-like design of active material, the hierarchical $\text{CoP}/\text{Ni}_5\text{P}_4/\text{CoP}$ microsheet arrays electrode shows Pt-like activity for HER with pH universality and exceptional stability. In 0.5 M H_2SO_4 , it requires overpotentials of only 33 and 85 mV to achieve current densities of 10 and 100 mA cm^{-2} , respectively, with a relatively small Tafel slope of 43 mV dec^{-1} and large exchange current density of 1.708 mA cm^{-2} , and exhibits large surface area and simultaneous high turnover frequencies (TOF) of 0.453 and 1.22 $\text{H}_2 \text{ s}^{-1}$ at 75 and 100 mV overpotentials, respectively, outperforming most efficient non-noble-metal HER electrocatalysts reported so far. In particular, this robust catalyst shows excellent durability at high current density of 1 A cm^{-2} . Moreover, the as-prepared $\text{CoP}/\text{Ni}_5\text{P}_4/\text{CoP}$ microsheet arrays electrode only requires 71 mV to deliver 10 mA cm^{-2} in 1M KOH, and also exhibits good durability at 30 and 500 mA cm^{-2} , demonstrating its pH universality for efficient hydrogen production.

The synthesis of the CoP catalyst involves three-step process as illustrated in Fig. 1. First, nickel (Ni) foam was thermally phosphorized at 500 °C in a tube furnace using red phosphorous (P) to form nickel phosphide nanosheet arrays,²⁰ as demonstrated by the scanning electron microscopy (SEM) images in Fig. 1b and 1f. Second, the nickel phosphide nanosheet arrays on Ni foam was soaked in the Co-ink and dried at ambient condition (Fig. 1c). The cobalt (Co) precursor ink was prepared by dissolving cobalt nitrate hexahydrate [$\text{Co}(\text{NO}_3)_2 \cdot 6\text{H}_2\text{O}$] in N,N-Dimethylformamide (DMF). The firmly constructed structure (Fig. 1b and 1f) as well as hydrophilic nature of the nickel phosphide nanosheets facilitated to develop a uniform coverage of the nanosheets by Co precursor ink. Finally, the dried sample was thermally phosphorized again at 500 °C, leading to the formation of a unique structure of hierarchical $\text{CoP}/\text{Ni}_5\text{P}_4/\text{CoP}$ microsheet arrays electrode, as revealed by the SEM images in Fig. 1d and 1g.

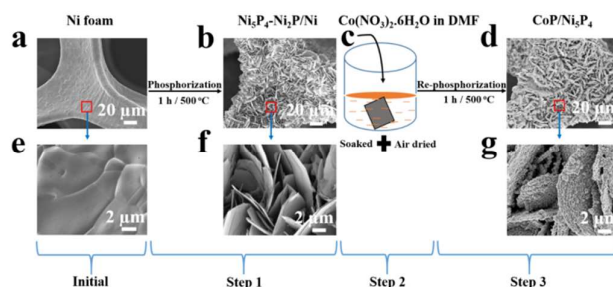


Fig. 1. Synthetic scheme of sandwich-like $\text{CoP}/\text{Ni}_5\text{P}_4/\text{CoP}$ electrocatalyst. (a,e) SEM images of Ni foam used as the starting electrode material. (b,f) SEM images of nickel phosphide nanosheet arrays after the first synthetic step. (c) Diagram showing nickel phosphide nanosheets on Ni foam that was soaked in cobalt precursor ink prepared by dissolving cobalt nitrate hexahydrate [$\text{Co}(\text{NO}_3)_2 \cdot 6\text{H}_2\text{O}$] in DMF. (d,g) SEM images of hierarchical $\text{CoP}/\text{Ni}_5\text{P}_4/\text{CoP}$ microsheet arrays after the third synthetic step.

The surface morphology of $\text{CoP}/\text{Ni}_5\text{P}_4/\text{CoP}$ microsheet arrays electrode changes greatly with varying the concentration of precursor Co-ink (Fig. S1, ESI[†]). With precursor ink concentration of 0.25 g/ml, most of the nickel phosphide nanosheets were uniformly covered by CoP after phosphorization (Fig. S1b, e, ESI[†]), leading to an extremely large surface exposure of the cobalt phosphide, and forming a sandwich-like structure between CoP nanoparticles and Ni_5P_4 nanosheet as confirmed by the SEM image (Fig. S2, ESI[†]). When the concentration was increased to 0.4 g/ml, all the interspaces between the nanosheets were filled by cobalt precursor, and the nickel phosphide nanosheets were buried (Fig. S1a, d, ESI[†]), thereby reducing the exposed surface of CoP. On the other hand, at very low concentration of the precursor ink (0.1 g/ml), most part of the nickel phosphide nanosheets were not covered by CoP (Fig. S1c, f, ESI[†]). Since the optimum coverage of the nickel phosphide nanosheets was achieved at Co precursor ink concentration of 0.25 g/ml, further analyses were carried out using this concentration unless otherwise mentioned. Meanwhile, in order to examine the role of phosphorus, a sample was also prepared by annealing in the absence of phosphorus source at the third step for comparison. A notably different morphology was observed in the absence of phosphorus source (Fig. S3a, b, ESI[†]), which may be due to the formation of different chemical compound of cobalt. In addition, the morphology varying with temperature was also investigated by phosphorization at 600 °C at the third step of synthesis. At 600 °C, a prominent change in surface structure of the CoP was demonstrated by SEM images in Fig. S4 (ESI[†]), which is due to structural deformation of inner frame of nickel phosphide nanosheets as well as outer cobalt phosphide coverage at higher temperature.

High resolution SEM images in Fig. 2a–c display closer view of the surface morphology of the CoP, demonstrating a porous structure of interconnected nanostructures composed of macropores from Ni foam and nickel phosphide nanosheets, and mesopores from CoP particles (Fig. S5 and S6, ESI[†]), which may contribute to the excellent HER catalytic activity by facilitating exposure of numerous active sites, and also offering efficient diffusion channels during H_2 evolution in water splitting. In order to gain further insight into the crystalline structure, the as-prepared electrocatalyst was examined

by transmission electron microscopy (TEM) (Fig. 2d-f). The high-resolution transmission electron microscopy (HRTEM) image in Fig. 2d clearly demonstrates that the nickel phosphide nanosheets are highly crystallized with the lattice fringe spacings of 0.207 nm and 0.298 nm corresponding to the (224) and (020) planes of Ni_5P_4 crystals, respectively. Accordingly, the outer coverage of the electrode indicates a mixed structure showing that a small fraction is crystallized corresponding to the (220) and (121) planes of CoP crystals, respectively, along with amorphous CoP as revealed by HRTEM images in Fig. 2e and 2f. Furthermore, the energy dispersive spectroscopy (EDS) elemental mapping confirms the uniform distribution of Co and P along with a small fraction of Ni, with atomic ratio of Co:P to be 1:0.93, which is very close to the 1:1 ratio as CoP, indicating the formation of CoP in the as-prepared electrode (Fig. S7, ESI[†]). The small fraction of Ni in the EDS mapping could be either from Ni_5P_4 that remained while peeling off the cobalt phosphide from the electrode during TEM sample preparation or from diffusion of Ni from inner support during synthesis.

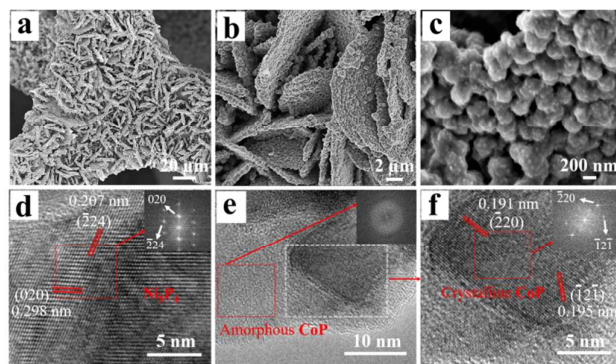


Fig. 2. Morphology and chemical composition of $\text{CoP}/\text{Ni}_5\text{P}_4/\text{CoP}$ electrocatalyst. (a-c) Typical SEM images of $\text{CoP}/\text{Ni}_5\text{P}_4/\text{CoP}$ electrode. (d) HRTEM image showing crystalline Ni_5P_4 at the inner structure of $\text{CoP}/\text{Ni}_5\text{P}_4/\text{CoP}$ electrode. The Fast Fourier Transform (FFT) in the inset demonstrates the crystal structure of Ni_5P_4 . (e, f) HRTEM images showing amorphous as well as crystalline CoP at the outer structure of $\text{CoP}/\text{Ni}_5\text{P}_4/\text{CoP}$ electrode. The FFTs in the inset of (e) and (f) demonstrate the amorphous and crystalline structures of CoP, respectively.

Powder X-ray diffraction (XRD) was employed to further characterize the phase composition of the samples and to determine the rough atomic ratio of different elements. Typical XRD patterns from the as-prepared nanosheet arrays after step 1 demonstrate a mixture of nickel phosphides: mainly Ni_5P_4 , minor Ni_2P and a small amount of metallic Ni (Fig. 3a), suggesting that the original Ni foam was not fully transformed to nickel phosphide. Interestingly, the XRD pattern of the electrode prepared with re-phosphorization after step 3, shows mostly Ni_5P_4 , along with a small shoulder around 48° of the 2-theta position corresponding to the CoP phase. The disappearance of Ni_2P and Ni after re-phosphorization may result from the diffusion of P source into the nickel and nickel phosphide converting them to Ni_5P_4 phase. To support this statement, we carried out a second phosphorization of nickel phosphide nanosheet samples in the same conditions as that of CoP growth. The XRD pattern (Fig. S8, ESI[†]) is the same as that of Ni_5P_4 crystals, confirming the conversion of mixed $\text{Ni}_5\text{P}_4/\text{Ni}_2\text{P}/\text{Ni}$

phases to a high-purity Ni_5P_4 phase during CoP growth. On the other hand, the small peak of CoP in XRD patterns indicates the presence of only a small fraction of CoP crystals and the rest could be amorphous CoP or simply because of the very thin thickness of CoP on top of Ni_5P_4 , further supporting the mixed composition of CoP in the as-prepared hierarchical $\text{CoP}/\text{Ni}_5\text{P}_4/\text{CoP}$ electrode as revealed by HRTEM images. In addition, compared to the nickel phosphide in the inner support structure, similar phase composition was noticed on the sample prepared by annealing only at the third synthetic step (Fig. S9, ESI[†]), which indicates no further phase change of the nickel rich phosphides in the absence of additional P source. Moreover, absence of shoulder in the XRD patterns around 48° of the 2-theta angular position for the sample prepared with annealing only, further supports that the small shoulder for the sample prepared with re-phosphorization during the third synthetic step is from the CoP crystals.

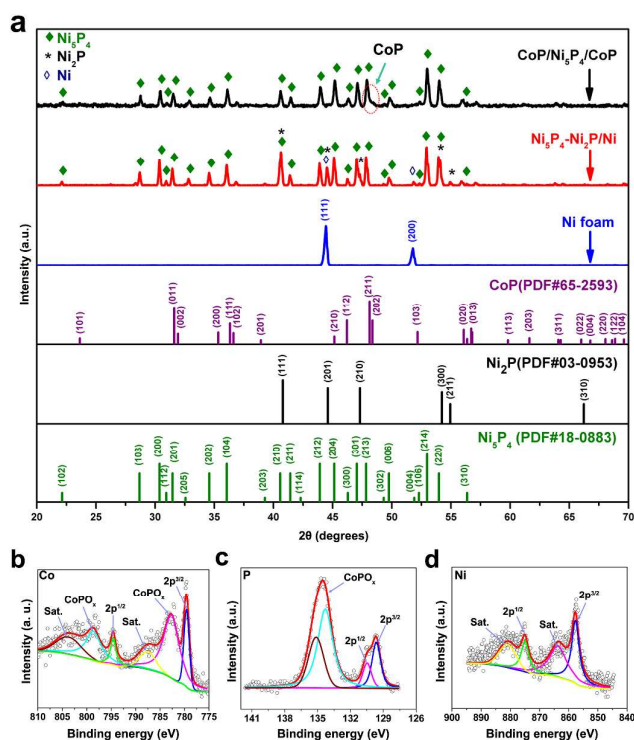


Fig. 3. Characterization of the $\text{CoP}/\text{Ni}_5\text{P}_4/\text{CoP}$ microsheet arrays electrode. (a) Typical XRD patterns showing the phase structure of Ni foam, $\text{Ni}_5\text{P}_4\text{-Ni}_2\text{P}/\text{Ni}$ support and $\text{CoP}/\text{Ni}_5\text{P}_4/\text{CoP}$ electrode. Detailed XPS analysis of: (b) Co 2p, (c) P 2p, and (d) Ni 2p spectra.

X-ray photoelectron spectroscopy (XPS) was utilized to study the surface chemical composition of the samples. According to the high-resolution XPS spectra of the hierarchical $\text{CoP}/\text{Ni}_5\text{P}_4/\text{CoP}$ arrays electrode, we can easily identify the presence of Co, P, and Ni (Fig. 3b-d, Fig. S10 and Table S1, ESI[†]). The Co core level peaks (Fig. 3b) appear at binding energies (BEs) of 779.6 eV and 794.6 eV, corresponding to Co $2p_{3/2}$ and $2p_{1/2}$ of cobalt phosphide,¹⁴ respectively. In the XPS spectra of Co 2p, some contribution from oxidized component of cobalt phosphide is also observed at BEs of 782.7 eV and 798.6 eV, corresponding to the $2p_{3/2}$ and $2p_{1/2}$,¹⁴ respectively. The P core level peaks (Fig. 3c) are located at 129.6 eV

and 130.5 eV, which correspond to the P 2p^{3/2} and 2p^{1/2} of CoP,^{14,16} respectively. In the XPS spectra of P 2p, peaks at BEs of 134.3 eV and 135.1 eV correspond to the oxidized state 2p^{3/2} and 2p^{1/2}, respectively, originating from the surface oxidation of the CoP.^{13,14,20,21} In addition, Ni core level peaks (Fig. 3d) are also observed at the BEs of 857.7 eV and 875.0 eV, originating from the Ni 2p^{3/2} and 2p^{1/2} of surface oxidized nickel phosphide,^{22,23} respectively, which is possibly from the protruded nickel phosphide nanosheets (Fig. S11, ESI[†]). The protruded part is possibly resulted from the formation of P-rich nickel phosphide (Ni₅P₄) phases by diffused P during re-phosphorization, and such feature is observed only in a few regions of the electrode. Furthermore, the BE of Co 2p centered at 779.6 eV is positively shifted from the position of elemental Co (778.1–778.2 eV), and that of P 2p centered at 129.6 eV is negatively shifted from the position of elemental P (129.9 eV), which imply that the Co carries a partial positive charge (δ^+) and the P carries a partial negative charge (δ^-) in CoP.^{14,24} This metal center Co (δ^+) and pendant base P (δ^-) in CoP resembles with hydrogenases and other metal complex HER catalysts, indicating the similar catalytic mechanism of CoP with them.^{25,26}

The electrochemical HER performance of the as-prepared electrocatalyst was first assessed in 0.5 M H₂SO₄, and a scan rate of 2 mV s⁻¹ was set to collect the polarization curves by linear sweep voltammetry in a three-electrode setup (Fig. S12, ESI[†]).²⁷ All the potentials used here were converted to the reversible hydrogen electrode (RHE). Fig. 4a presents the relevant polarization curves of

different electrodes including hierarchical CoP/Ni₅P₄/CoP microstructured arrays, pure Ni foam, a Pt wire, and the Ni₅P₄-Ni₂P/Ni nanosheet arrays support. The CoP/Ni₅P₄/CoP electrocatalyst shows a fast increase of cathodic current density with increasing overpotentials, suggesting CoP/Ni₅P₄/CoP as a high-performance 3D cathode for hydrogen generation from water splitting. At a geometric current density of 10 mA cm⁻², the as-prepared hierarchical CoP/Ni₅P₄/CoP 3D electrode requires an overpotential of only 33 mV, which is very close to that of Pt (31 mV), and much lower than 293 mV for pure Ni foam and 79 mV for the Ni₅P₄-Ni₂P/Ni support. Compared to the samples prepared with 0.4 and 0.1 g/ml concentration of precursor Co-ink at the second synthetic step, the sample prepared with 0.25 g/ml exhibits much better electrocatalytic performance (Fig. S13, ESI[†]), which is possibly due to the greater exposure of active surface as revealed by SEM images in Fig. S1b and S1e. In contrast, the catalytic activity of the sample prepared by annealing only at the step 3 of synthesis shows a poorer HER performance (Fig. S14, ESI[†]) similar to the Ni₅P₄-Ni₂P/Ni support, possibly due to the formation of cobalt oxide rather than cobalt phosphide in the absence of P source. This oxide is not stable during water electrolysis as supported by the SEM images taken after electrochemical test (Fig. S3c, ESI[†]), which shows that the outer layer of cobalt compound was washed away by highly corrosive acidic electrolyte during electrochemical potential cycling, leaving behind the nickel phosphide nanosheet arrays skeleton.

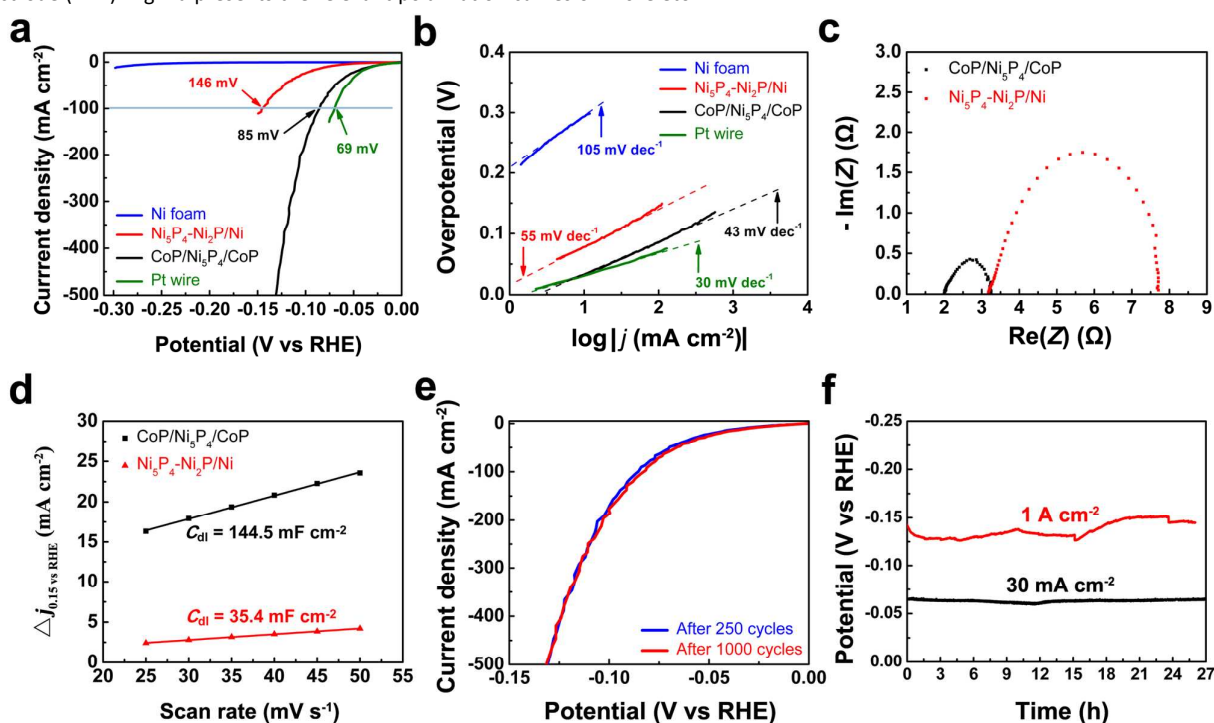


Fig. 4. Electrochemical measurements of different electrodes for hydrogen evolution in acid. (a) The polarization curves of the CoP/Ni₅P₄/CoP, Ni₅P₄-Ni₂P/Ni, pure Ni foam, and a Pt wire electrodes. (b) Tafel plots derived from the curves in (a). (c) EIS Nyquist plots of the CoP/Ni₅P₄/CoP and Ni₅P₄-Ni₂P/Ni electrodes. (d) The double-layer capacitance (C_{dl}) of the CoP/Ni₅P₄/CoP and Ni₅P₄-Ni₂P/Ni electrodes. (e) Polarization curves of the CoP/Ni₅P₄/CoP electrode after 250 and 1000 cycles. (f) Potential testing at constant current densities of 30 mA cm⁻² and 1 A cm⁻² on the CoP/Ni₅P₄/CoP electrode.

On the other hand, the phosphorization temperature at step 3 of synthesis plays an important role in the morphologies of the hierarchical CoP/Ni₅P₄/CoP, which accordingly has great effects on the electrocatalytic HER activity, confirming that 500 °C is the optimal temperature for growing this sandwich-like CoP/Ni₅P₄/CoP electrocatalyst (Fig. S15, ESI[†]). Especially, the electrocatalytic performance of CoP/Ni₅P₄/CoP grown at 500 °C is much better than many of the highly efficient HER electrocatalysts reported recently (Table S2, ESI[†]), including nanostructured Ni₂P (105 mV),¹⁰ Mo-W-P/carbon cloth (100 mV),¹³ WS₂(1-x)Se_{2x}/NiSe₂ (88 mV),²⁸ MoS₂(1-x)Se_{2x}/NiSe₂ (69 mV),²⁹ CoP/carbon cloth (67 mV),¹⁴ Ni/Ni₅P₄/NiP₂ (61 mV),¹⁸ CoNiP (60 mV),³⁰ CoPS (48 mV),¹⁵ Fe_{0.5}Co_{0.5}P (37 mV),¹⁶ etc. In addition, a Tafel slope of 43 mV dec⁻¹ (Fig. 4b), derived from the polarization curve, indicates that the HER process by this CoP/Ni₅P₄/CoP electrode proceeds through Volmer-Heyrovský mechanism.³¹ Moreover, from the relevant Tafel plot, we can extract the exchange current density to be 1.708 mA cm⁻² for the CoP/Ni₅P₄/CoP catalyst (Table S2, ESI[†]), which is significantly larger than most of the reported active catalysts based on transition metal chalcogenides including CoSe₂,⁹ WP₂ nanowire/CC,³² and transition metal phosphides including CoP,¹⁴ Ni₂P¹⁰, and MoP particles.³³ Finally, to further explore the superior catalytic performance of this sandwich-like catalyst, we quantified its TOF values at different overpotentials using a normal electrochemical method (Fig. S16, ESI[†]). This parameter is a very important performance index representing the intrinsic catalytic activity of the catalyst. As shown in Table S3 (ESI[†]), the TOF values are evaluated to be around 0.453 and 1.220 H₂ s⁻¹ at overpotentials of 75 and 100 mV, respectively. Especially, this TOF value increases to 4 H₂ s⁻¹ at only 135 mV (Fig. S17, ESI[†]). Thus, this sandwich-like CoP/Ni₅P₄/CoP is found to have a very low overpotential (33 mV), small Tafel slope (43 mV dec⁻¹), extremely large exchange current density (1.708 mA cm⁻²), and very large TOF value of 4 H₂ s⁻¹ at 135 mV, suggesting its exceptional H₂-evolving efficiency.

The physical origin of the electrode kinetics was further examined by electrochemical impedance spectroscopy (EIS) at the potential of -0.150 V vs RHE, and the EIS Nyquist plots (Fig. 4c) can be well fitted by a simplified Randles circuit (Fig. S18, ESI[†]). The series (*R_s*) and charge-transfer resistances (*R_{ct}*) are extracted from the fitted plots. Obviously, the *R_{ct}* of the CoP/Ni₅P₄/CoP microsheet arrays electrode is 1.2 Ω, meaning very fast charge transfer between the electrolyte and the catalyst. Also, there is a small *R_s* (2.0 Ω) for this catalyst, which reflects strong electrical integration of the catalyst to its support. To unveil the difference of intrinsic catalytic activity between Ni₅P₄-Ni₂P/Ni support and CoP/Ni₅P₄/CoP microsheet arrays (Table S4, ESI[†]), we adopted a cyclic voltammetry (CV) method (Fig. 4d, Fig. S19, ESI[†]) to derive the electrochemical double-layer capacitance (*C_{dl}*),^{20,29,34} which is directly related to the electrochemically active surface area (ECSA) of the electrocatalysts. Obviously, there is a large electrochemical surface area and roughness factor due to the presence of mesopores, nanosheet arrays and macropores of the catalyst (Table S3, ESI[†]). Then the exchange current density (*j_{0,normalized}*) is further normalized by the *C_{dl}* values, which is a useful parameter to compare the intrinsic catalytic activity. After normalization (Table S4, ESI[†]), we find that the normalized exchange current density of this CoP/Ni₅P₄/CoP catalyst is 625.6 μA cm⁻², which is still far larger

than that (366.1 μA cm⁻²) of the Ni₅P₄-Ni₂P/Ni support, demonstrating that the CoP/Ni₅P₄/CoP catalyst has a higher intrinsic catalytic activity than Ni₅P₄-Ni₂P/Ni nanosheet arrays-based catalyst. The exchange current density of the as-prepared CoP/Ni₅P₄/CoP catalyst compares favorably to most of the highly efficient electrocatalysts reported so far (Table S2, ESI[†]). Thus, according to the *C_{dl}* measurements and EIS analysis, the CoP/Ni₅P₄/CoP electrode has a much higher electrode kinetics toward hydrogen evolution, which could be related to the following factors: (1) The strong contact of CoP with inner Ni₅P₄ support that enables good mechanical and electrical connection, providing an easy pathway for electrons to flow during cathodic polarization. (2) Excellent electrical conductivity of CoP, facilitating fast charge transport. (3) The 3D structure along with highly porous feature of the interconnected nanostructures that enables greater exposure of active sites for hydrogen adsorption as well as easy diffusion pathways for the electrolyte and gaseous products.³⁵

Durability is another important factor to assess the electrocatalysts, which was studied by conducting accelerated cyclic voltammetry between potentials of 0.050 V and -0.150 V vs RHE at a scan rate of 50 mV s⁻¹ for 1000 potential cycles. No significant reduction in the current densities (Fig. 4e) demonstrated the excellent operational stability of the as-prepared catalyst. Also, we performed chronopotentiometry test at two different current densities of 30 mA cm⁻² and 1 A cm⁻² for over 25 hours (Fig. 4f). No dramatic change of the potential is detected, further confirming the exceptional operational stability of the CoP/Ni₅P₄/CoP catalyst in acid at a very high current density. Additionally, we examined the structure, phase and surface chemical composition of the electrocatalyst after performing 1000 CV cycles polarization test by SEM, XRD, and XPS (Fig. S20-S22, ESI[†]). Evidently, almost no obvious changes are found in the SEM images and XRD patterns, meaning that there is no change of the crystal structure and phase of the catalysts during HER testing. The XPS spectra of Co 2p and P 2p core level peaks of CoP/Ni₅P₄/CoP electrode after electrochemical test showed almost diminished peaks from oxides, possibly due to the reduction of surface oxidation during potential cycles.

The CoP/Ni₅P₄/CoP electrocatalyst also demonstrates promising HER activity under alkaline condition. Fig. 5 shows the HER performance of CoP/Ni₅P₄/CoP in 1.0 M KOH (pH=14). The hierarchical CoP/Ni₅P₄/CoP requires only 71 and 140 mV of overpotentials to obtain the current densities of 10 and 100 mA cm⁻², respectively, along with the Tafel slope of 58 mV dec⁻¹. The catalytic activity of as-prepared CoP/Ni₅P₄/CoP is relatively inferior to that of Pt at benchmark current density of 10 mA cm⁻² in alkaline media, however, it compares favorably to the recently reported efficient non-noble-metal based HER catalysts, including NiS₂/MoS₂ (204 mV),³⁶ transition metal phosphides (Table S5, ESI[†]) CoMoP (81 mV),³⁷ (Co_{1-x}Fe_x)₂P (79 mV),³⁸ etc. We further investigated the electrochemical performance at large current densities (Fig. 5a). Interestingly, the CoP/Ni₅P₄/CoP electrode shows more efficient catalytic activity than the Pt wire at current density higher than 91 mA cm⁻², which is very important for large scale hydrogen production *via* water electrolysis.

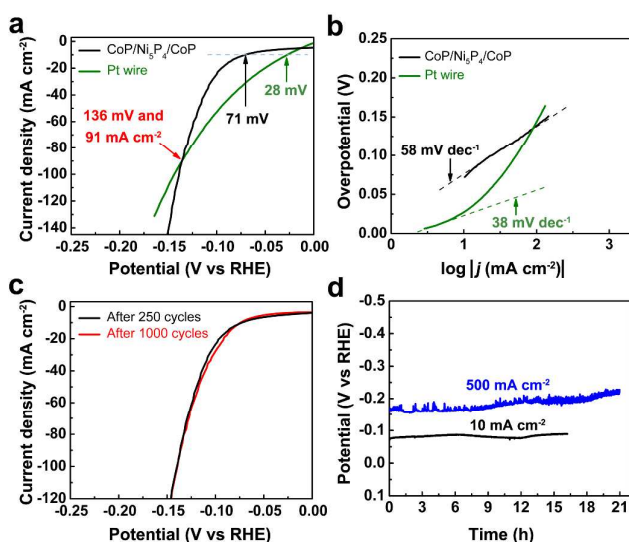


Fig. 5. Electrochemical performance of CoP/Ni₅P₄/CoP microsHEET arrays electrode in 1.0 M KOH. (a) Polarization curves recorded on CoP/Ni₅P₄/CoP and a Pt wire. (b) Tafel plots of the catalysts in (a). (c) Polarization curves of the CoP/Ni₅P₄/CoP electrode after 250 and 1000 cycles. (d) Chronopotentiometry tests at 10 and 500 mA cm⁻².

Although the CoP/Ni₅P₄/CoP shows inferior HER performance to some binary metal-based electrocatalysts including MoNi₄ (15 mV at 10 mA cm⁻²)³⁹ and NiCoP (32 mV at 10 mA cm⁻²)⁴⁰ in the alkaline electrolyte, its pH-universal HER activity in a wide pH range is very compelling. Especially, it is noticed that metal phosphosulfides are promising electrocatalysts for hydrogen generation from water splitting in acid or base,^{15,41} however, the best catalyst still requires an overpotential of 48 mV to reach the benchmark current density 10 mA cm⁻² in acid,¹⁵ which is not so efficient as ours (33 mV). A recently reported heterogeneous catalyst based on bimetallic phosphide/sulfide has been reported to have great potential as a bifunctional catalyst for overall water splitting in base, but it shows catalytic HER activity inferior to ours.⁴¹ Our catalyst has much lower Tafel slope, faster increase of the geometric current density with the overpotential, lower overpotential (71 mV) to reach 10 mA cm⁻², and especially promising for hydrogen generation at wide pH ranges. Furthermore, the reasonable operational stability at high current density in highly alkaline medium as well (Fig. 5d), is another important feature of the as-prepared electrode that may be of great potential to be implemented as a sustainable pH universal hydrogen evolving electrode. Finally, the gas products and relevant Faradaic efficiency were evaluated in acid and base electrolytes by the gas chromatography-based technique²⁹ (Fig. S23, ESI[†]). The efficiency, which reflects the conversion of the electrons involved in the catalytic reaction, is determined to be nearly 100%, meaning that nearly all the electrons are utilized for generating H₂ during water electrolysis.

Conclusions

In conclusion, a highly efficient HER electrocatalyst is developed with a facile synthetic approach. The as-prepared hierarchical CoP/Ni₅P₄/CoP microsHEET arrays electrode is binder free, self-

supported 3D architecture that can be directly used as a cathode for HER. The CoP/Ni₅P₄/CoP microsheets arrays electrode shows Pt-like activity for HER catalysis with reasonable operational stability at high current density in acidic as well as alkaline electrolytes. The outstanding HER catalytic activity of this electrode is related to the good mechanical and electrical connection between CoP catalyst and Ni₅P₄ support, numerous active sites and high intrinsic catalytic activity of the sandwich-like CoP/Ni₅P₄/CoP electrode. We believe that our study will open up a new exciting avenue to explore the design of self-supported 3D robust HER catalysts for large-scale hydrogen production *via* water splitting.

Acknowledgements

This project was supported by US Department of Energy under a grant DE-SC0010831. S. C. also likes to thank the support from TcSUH as the TcSUH Robert A. Welch Professorships in High Temperature Superconducting (HTSg) and Chemical Materials (E-0001).

References

- 1 N. Armaroli and V. Balzani, *Angew. Chem. Int. Ed.*, 2007, **46**, 52-66.
- 2 J. O. M. Bockris, *Int. J. Hydrogen Energy*, 2002, **27**, 731-740.
- 3 H. Q. Zhou, F. Yu, J. Y. Sun, R. He, S. Chen, C. W. Chu and Z. F. Ren, *Proc. Natl. Acad. Sci. U. S. A.*, 2017, **114**, 5607-5611.
- 4 I. Roger, M. A. Shipman and M. D. Symes, *Nat. Rev. Chem.*, 2017, **1**, 1-11.
- 5 R. B. Gordon, M. Bertram and T. E. Graede, *Proc. Natl. Acad. Sci., U.S.A.* 2006, **103**, 1209-1214.
- 6 M. S. Faber and S. Jin, *Energy Environ. Sci.*, 2014, **7**, 3519-3542.
- 7 H. Vrubel, D. Merki and X. L. Hu, *Energy Environ. Sci.*, 2012, **5**, 6136-6144.
- 8 L. Guo, Z. Yang, K. Marcus, Z. Li, B. Luo, L. Zhou, X. Wang, Y. Du and Y. Yang, *Energy Environ. Sci.*, 2018, **11**, 106-114.
- 9 D. Kong, H. Wang, Z. Lu and Y. Cui, *J. Am. Chem. Soc.*, 2014, **136**, 4897-4900.
- 10 E. J. Popczun, J. R. McKone, C. G. Read, A. J. Biech, A. M. Wiltrout, N. S. Lewis and R. E. Schaak, *J. Am. Chem. Soc.*, 2013, **135**, 9267-9270.
- 11 P. Xiao, W. Chen and X. Wang, *Adv. Energy Mater.*, 2015, **5**, 1500985.
- 12 Y. M. Shi and B. Zhang, *Chem. Soc. Rev.*, 2016, **45**, 1529-1541.
- 13 X. D. Wang, Y. F. Xu, H. S. Rao, W. J. Xu, H. Y. Chen, W. X. Zhang, D. B. Kuang and C. Y. Su, *Energy Environ. Sci.*, 2016, **9**, 1468-1475.
- 14 J. Tian, Q. Liu, A. M. Asiri and X. P. Sun, *J. Am. Chem. Soc.*, 2014, **136**, 7587-7590.
- 15 M. C. Acevedo, M. L. Stone, J. R. Schmidt, J. G. Thomas, Q. Ding, H. C. Chang, M. L. Tsai, J. H. He and S. Jin, *Nat. Mater.*, 2015, **14**, 1245-1251.
- 16 C. Tang, L. F. Gan, R. Zhang, W. B. Lu, X. Jiang, A. M. Asiri, X. P. Sun, J. Wang and L. Chen, *Nano Lett.*, 2016, **16**, 6617-6621.
- 17 J. Mahmood, F. Li, S. M. Jung, M. S. Okyay, I. Ahmad, S. J. Kim, N. Park, H. Y. Jeong and J. B. Baek, *Nat. Nanotechnol.* 2017, **12**, 441-446.
- 18 Z. Peng, D. Jia, A. M. Al-Enizi, A. A. Elzatahry and G. Zheng, *Adv. Energy Mater.*, 2015, **5**, 1402031.

- 19 A. Kundu, J. N. Sahu, G. Redzwan and M. A. Hashim, *Int. J. Hydrogen Energy*, **2013**, *38*, 1745-1757.
- 20 I. K. Mishra, H. Q. Zhou, J. Y. Sun, K. Dahal, Z. S. Ren, R. He, S. Chen and Z. F. Ren, *Mater. Today Phys.*, **2018**, *4*, 1-6.
- 21 E. J. Popczun, C. G. Read, C. W. Roske, N. S. Lewis and R. E. Schaak, *Angew. Chem. Int. Ed.*, **2014**, *53*, 5427-5430.
- 22 M. Ledendecker, S. K. Calderón, C. Papp, H. P. Steinrück, M. Antonietti and M. Shalom, *Angew. Chem. Int. Ed.*, **2015**, *54*, 12361-12365.
- 23 Y. Q. Sun, L. F. Hang, Q. Shen, T. Zhang, H. L. Li, X. M. Zhang, X. J. Lyu and Y. Li, *Nanoscale* **2017**, *9*, 16674-16679.
- 24 A. P. Grosvenor, S. D. Wik, R. G. Cavell and A. Mar, *Inorg. Chem.*, **2005**, *44*, 8988-8998.
- 25 Y. Nicolet, A. L. de Lacey, X. Vernède, V. M. Fernandez, E. C. Hatchikian and J. C. Fontecilla-Camps, *J. Am. Chem. Soc.*, **2001**, *123*, 1596-1601.
- 26 P. Liu and J. A. Rodriguez, *J. Am. Chem. Soc.*, **2005**, *127*, 14871-14878.
- 27 S. Anantharaj, S. R. Ede, K. Karthick, S. Sam Sankar, K. Sangeetha, P. E. Karthik and Subrata Kundu, *Energy Environ. Sci.*, **2018**, *11*, 744-771.
- 28 H. Q. Zhou, F. Yu, J. Y. Sun, H. T. Zhu, I. K. Mishra, S. Chen and Z. F. Ren, *Nano Lett.*, **2016**, *16*, 7604-7611.
- 29 H. Q. Zhou, F. Yu, Y. F. Huang, J. Y. Sun, Z. Zhu, R. J. Nielsen, R. He, J. M. Bao, W. A. Goddard III, S. Chen and Z. F. Ren, *Nat. Commun.*, **2016**, *7*, 12765.
- 30 A. L. Han, H. L. Chen, H. Y. Zhang, Z. J. Sun and P. W. Du, *J. Mater. Chem. A*, **2016**, *4*, 10195-10202.
- 31 Y. Yang, H. L. Fei, G. D. Ruan, C. S. Xiang and J. M. Tour, *Adv. Mater.*, **2014**, *26*, 8163-8168.
- 32 M. Y. Pi, T. L. Wu, D. Zhang, S. J. Chen and S. X. Wang, *Nanoscale*, **2016**, *8*, 19779-19786.
- 33 P. Xiao, M. A. Sk, L. Thia, X. M. Ge, R. J. Lim, J. Y. Wang, K. H. Lim and X. Wang, *Energy Environ. Sci.*, **2014**, *7*, 2624-2629.
- 34 J. Kibsgaard and T. F. Jaramillo, *Angew. Chem. Int. Ed.*, **2014**, *53*, 14433-14437.
- 35 H. W. Liang, X. D. Zhuang, S. Brüller, X. L. Feng and K. Müllen, *Nat. Commun.*, **2014**, *5*, 4973.
- 36 P. Y. Kuang, T. Tong, K. Fan and J. G. Yu, *ACS Catal.*, **2017**, *7*, 6179-6187.
- 37 Y. Y. Ma, C. X. Wu, X. J. Feng, H. Q. Tan, L. K. Yan, Y. Liu, Z. H. Kang, E. B. Wang and Y. G. Li, *Energy Environ. Sci.*, **2017**, *10*, 788-798.
- 38 Y. W. Tan, H. Wang, P. Liu, Y. H. Shen, C. Cheng, A. Hirata, T. Fujita, Z. Tang and M. W. Chen, *Energy Environ. Sci.*, **2016**, *9*, 2257-2261.
- 39 J. Zhang, T. Wang, P. Liu, Z. Q. Liao, S. H. Liu, X. D. Zhuang, M. W. Chen, E. Zschech and X. L. Feng, *Nat. Commun.*, **2017**, *8*, 15437.
- 40 H. F. Liang, A. N. Gandhi, D. H. Anjum, X. B. Wang, U. Schwingenschlögl and H. N. Alshareef, *Nano Lett.*, **2016**, *16*, 7718-7725.
- 41 Y. M. Xin, X. Kan, L. Y. Gan and Z. H. Zhang, *ACS Nano*, **2017**, *11*, 10303-10312.



Energy & Environmental Science

Paper

The table of contents entry

Exceptional Pt-like electrocatalytic activity was achieved in sandwich-like catalyst of CoP/Ni₅P₄/CoP microsHEET arrays for pH-universal hydrogen evolution by simply wrapping Ni₅P₄ nanosheet arrays with CoP nanoparticles.

TOC figure

